DE-FG22-96PC96223--04

"SURFACTANT - POLYMER INTERACTION FOR IMPROVED OIL RECOVERY"

DISCLAIMER

"SURFACTANT-POLYMER INTERACTION IN ENHANCED OIL RECOVERY"

ABSTRACT

The goal of this research is to use the interaction between a surfactant and a polymer for efficient displacement of tertiary oil by improving slug integrity, adsorption and mobility control. Surfactant - polymer flooding has been shown to be highly effective in laboratory-scale linear floods. The focus of this proposal is to **design an inexpensive surfactant-polymer mixture that can efficiently recover tertiary oil** by avoiding surfactant slug degradation, high adsorption and viscous/heterogeneity fingering.

A mixture comprising a "pseudo oil" with appropriate surfactant and polymer has been selected to study micellar-polymer chemical flooding. The physical properties and phase behavior of this system have been determined. A surfactant-polymer slug has been designed to achieve high efficiency recovery by improving phase behavior and mobility control. Recovery experiments have been performed on linear cores and a quarter 5-spot. The same recovery experiments have been simulated using a commercially available simulator (UTCHEM). Good agreement between experimental data and simulation results has been achieved.

"SURFACTANT - POLYMER INTERACTION FOR IMPROVED OIL RECOVERY"

TABLE OF CONTENTS

"SURFACTANT-POLYMER INTERACTION IN ENHANCED OIL RECOVERY"

EXECUTIVE SUMMARY

A research project is proposed to develop new polymer/surfactant blends for use in oil field production and improved oil recovery operations. These operations include fingering reduction and improved oil recovery by polymer-surfactant flooding.

The group carrying out this project is comprised of researchers from the Chemical Engineering Department at Prairie View A&M University (PVAMU), a Historical Black College and University (HBCU), from the Chemical Engineering Department at the University of Houston (UH), and BDM Petroleum Technologies (BDMPT). The joint partnership offers unique advantages obtained from support to an HBCU of a major academic institution and a private company using advanced technologies and research facilities.

The research group at BDMPT reports experimental data about suitable oil-surfactant-polymer systems and their properties. The research group at UH carries out flow experiments using the aforementioned systems. The group at PVAMU computes stability phase maps and simulates the experiments at UH.

A vast amount of proven domestic oil deposit is stranded in reservoirs too shallow for miscible flooding, yet this oil is too light for thermal techniques. Surfactant-polymer flooding is the only method to unlock this vast resource. The integrity of the surfactant slug is critical to the economic success of a surfactant-polymer flood. This research supplies experimental data, phase maps and mechanistic principles for optimum surfactant-polymer slug-design.

"SURFACTANT - POLYMER INTERACTION FOR IMPROVED OIL RECOVERY"

INTRODUCTION

More than 224 billion barrels of immobile oil remain in U. S. domestic reservoirs. For a number of reservoirs, chemical IOR methods may be the only viable method for significantly reducing oil saturation in the field. The key to success of any chemical IOR method depends not only on the effectiveness of chemicals to mobilize residual crude oil, but also on ensuring that the treatments actually contact oil through appropriate use of profile modification treatments and on the ability of mobility control agents to move the oil to the production wells. New research is needed, especially in chemical flooding methods, to reduce the operation cost. Chemical IOR systems include surfactants, polymers, alkali agents, or combinations thereof. Surfactants and alkali agents can lower interfacial tension (IFT) between oil and water, thereby mobilizing the immobile oil. Alkali agents can also act to reduce surfactant losses from precipitation and adsorption. Polymers are used to viscosify aqueous solutions and maintain mobility control. Other types of polymer formulations are used to block high permeability zones and divert injection fluids to lower permeability, unswept zones. Several adverse polymer-surfactant interactions can occur, phase separations, precipitation, and loss of viscosity. The integrity of the surfactant slug is critical to the economic success of a surfactant-polymer flood.

The goal of the proposed research is to use the interaction between a surfactant and a polymer for efficient displacement of tertiary oil by improving slug integrity, adsorption and mobility control. The mobility ratio across surfactant - oil bank flood front is often unfavorable, but can be stabilized by the addition of polymers. The focus of this proposal is to **design an inexpensive surfactant-polymer mixture that can efficiently recover tertiary oil** by avoiding surfactant slug degradation, high adsorption and viscous/heterogeneity fingering.

This project is been carried out by a team involving, Dr. Kishore Mohanty from the University of Houston (UH), Dr. Jorge Gabitto from Prairie View A&M University (PVAMU) and Petroleum Technologies (BDM-PT). Dr. Mohanty performs the experimental work at UH, Dr. Gabitto conducts numerical simulation and theoretical studies and BDMPT performs experiments and provides data concerning the selection and physical properties of a suitable oil-surfactant-polymer system to be used in the experiments and numerical simulations.

TECHNICAL INTRODUCTION

BACKGROUND

For a big number of reservoirs, chemical EOR methods may be the only viable methods for significantly reducing oil saturation in the field.

Capillary forces cause large quantities of oil to be left behind after waterflooding of an oil reservoir. Capillary forces arise from the interfacial tension (IFT) between the oil and water phases that resist externally applied viscous forces and causes the injected water to bypass the resident oil. The predominant mechanism to recover this oil is lowering the IFT through the addition of suitable chemicals (surfactants). Lower interfacial forces recover additional oil by reducing these capillary forces. This trapping of the resident oil can be expressed as a competition between viscous forces, which mobilize the oil, and capillary forces, that trap the oil.

In practice surfactant injection alone can not achieve sufficient recovery due to several problems, fingering, adsorption, surfactant-soil interactions, etc. Therefore, a more complex process involving different steps is required to fully realize this technique potential. This recovery process receives different names, but throughout this work we will use the term micellar-polymer flooding (MP) following Lake[1].

Figure 1 (taken from Lake[1]), shows an idealized version of an MP flooding sequence. The process is applied in the drive mode. The process consists of:

Preflush. A volume of brine to lower salinity is added first. Preflushes range from 0 to 100% pore volume (PV). Sometimes an agent is added to lessen the surfactant retention[2].

MP slug. The main surfactant, cosurfactants, and other chemicals are added later. Slug volumes range from 5 to 20% PV.

Mobility buffer. This fluid is a dilute solution of a water-soluble polymer whose purpose is to drive the MP slug and banked-up fluids towards the production wells. The buffer volumes range from 0 to 100% PV.

Mobility buffer taper. This is a volume of brine that contains dilute polymer added to produce a gradual change in polymer concentration from the mobility buffer concentreation to zero.

Chase water. This fluid is injected to reduce the cost of continuous injection of polymer.

Adequate design of all these different steps requires careful consideration of phase behavior and physical properties of all the chemicals used. A successful MP flood must achieve three things for effective oil recovery[2].

(1). The MP slug should propagate at optimal conditions, especially salinity.

(2). Surfactant concentration should be big enough so that some of it is unretained by permeable surfaces.

(3). The active surfactant should sweep a large portion of the reservoir without excessive dissipation due to dispersion or channeling.

One of the most important variables to achieve the aforementioned conditions is salinity. It will later be shown that salinity significantly influence phase behavior and physical properties in an MP process. Lowering the resident salinity is the main purpose of the preflush step. A successful preflush will permit an MP slug to displace oil wherever it goes and will reduce retention and loss of surfactant activity. Several salinity gradient design techniques have been proposed[3,4]. The concept is to dynamically lower the resident salinity to optimal by injecting an underoptimal mobility buffer salinity. Pope et al.[5] found salinity to be the most important variable controlling the oil recovery process in a series of laboratory experiments.

Mobility control of the MP slug is another critical factor in achieving a successful recovery. Field slugs are relatively small and can not tolerate even a small amount of fingering. Therefore, a slug less mobile than the oil bank it is displacing is sought. Polymer should be added to the MP slug to achieve this goal. The spike portion of the mobility buffer must have a mobility equal or less than the slug. Since the slug mobility also depends upon the oil concentration, the slug and mobility buffer should be designed together.

SURFACTANT-BRINE-OIL PHASE BEHAVIOR

In other to understand the bases for a successful MP process design a simplified system phase behavior is presented. Surfactant-brine-oil is conventionally illustrated on a ternary diagram[1]. The top apex of the diagram represents the surfactant pseudo-component, the lower left represents the brine and the lower right represents oil (see Figure 2).

Brine salinity strongly affects the phase behavior. Figure 3 shows a sequence of phase diagrams as salinity is increased. The phase behavior described here has been taken from Nelson and Pope[6]. At low brine salinity, a typical surfactant will exhibit good aqueous-phase solubility and poor oil phase solubility. Thus an overall composition near the brine-oil boundary will split into two phases: an excess almost pure oil phase and a micro-emulsion phase that contains brine, surfactant and solubilized oil. This type of phase behavior is called Winsor type I or type II(-) system. We adopt the type II(-) terminology in this work. The two phase region is enclosed by a binodal curve. Equilibrium two phase compositions are linked by tie-lines. A especial point (plait) denotes the composition at which the concentrations in both phases coincide. Above the binodal curve we have only one phase. The tie-lines in II(-) behavior have negative slopes.

For high brine salinities electrostatic forces reduce the surfactant's solubility in the aqueous solution. Therefore, an overall composition, within the two-phase region, will split into an excess brine phase and a micro-emulsion phase that contains most of the surfactant and some solubilized brine. The phase environment is called a Winsor type II or a type II(+) system. These behaviors constitute extreme cases. For a range of

intermediate salinities a third surfactant rich phase can appear. An overall composition within the three-phase region separates into excesses oil and water rich phases and into a micro-emulsion phase whose composition is represented by an invariant point. This phase behavior is called a Winsor III type or a type III system. To the upper right and left of the three-phase region there are type II(-) and II(+) lobes wherein two phases will form as before. Type III behavior starts after a critical lower effective salinity (C_{Sel}) is reached[6]. The behavior disappears when critical upper effective salinity (C_{Seu}) is reached[6]. Over the type III salinity range there is migration of the invariant concentration point M from near the oil apex to near the brine apex. As the migration takes place the surfactant concentration in the microemulsion reaches a minimum when the oil-brine ratio at the invariant point becomes 1. The migration of the invariant point implies essentially unlimited solubility of oil and brine in a single phase. Several physical properties take extreme values at this critical point. This change in system's properties is used to determine optimal conditions for the recovery process. For example, there is a clear relationship between interfacial tension and phase behavior. The optimal salinity point can be determined by plotting interfacial tensions in the oil rich and aqueous rich phases versus salinity[7]. Fig.6 illustrates this behavior. The optimal salinity determined using interfacial tension agrees well with optimal salinities determined using other properties such as, solubilization ratios and oil recovery results. The optimal salinity corresponds roughly to the salinity where oil recovery from a core is maximum[1]. Optimal salinities depend upon the nature of the surfactant and the brine pseudo-components. Adding co-surfactants to the MP slug normally increases the optimal IFT. The notion of optimal salinity is directly related to the phase behavior of MP systems. Even properties such as, retention, are functions of salinity, co-surfactant concentration, and temperature. This observation leads to the speculation that all MP properties correlate to optimal salinity[1].

SIMULATOR BACKGROUND

UTCHEM, a chemical simulator developed by researchers at the University of Texas at Austin[8], has been used for the simulation program. UTCHEM is a multi-component, multiphase, three-dimensional compositional with variable temperature simulation model[8]. The basic equations are as follows:

1) the mass balance equations, which are solved up to 21 species;

2) the aqueous phase pressure, which is obtained by an overall mass balance on volume-occupying species (water, oil, surfactant, alcohol, and gas). The other phase pressures are computed by using the capillary pressures between phases;

3) the energy balance equation, which includes heat flow between the reservoir and the overburden rocks.

The flow equations allow for compressibility of rock and fluids, dispersion and molecular diffusion, chemical reactions, and phase behavior and are complemented by constitutive equations. The model includes options for multiple wells completed either horizontally or vertically. Aquifer boundaries are modeled as constant potential surfaces or as closed surfaces.

The flow equations are solved using a block-centered finite-difference scheme. The solution method is implicit in pressure and explicit in concentration (IMPES-like). Either one, two-point upstream, or third-order spatial, discretization is used. A brief description of the equations used in the code is provided below.

Mass Conservation Equations. The assumptions imposed when developing the flow equations are:

1) local thermodynamic equilibrium, except for tracers;
2) immobile solid phases;
3) slightly compressible rock and fluids;
4) Fickian dispersion;
5) ideal mixing; and
6) Darcy's law.

The boundary conditions are no flow and no dispersive flux across the impermeable boundaries.

The mass continuity for component k in association with Darcy's law is given in terms of overall volume of component k per unit pore volume ($\tilde{C}_k$) as,

$$\frac{\partial}{\partial t}\left(\phi\, \tilde{C}_k\, \rho_k\right) + \underline{\nabla} \bullet \sum_{j=1}^{n_p} r_k \left(C_{kj} u_j - \underline{\nabla} \bullet \underline{\underline{D}}\right) = R_k \qquad (1),$$

where the overall volume of component k is the summation over all phases including the adsorbed phases,

$$\tilde{C}_k = \left\{1 - \sum_{k=1}^{n_{cv}} \hat{C}_k\right\} \sum_{j=1}^{n_p} S_j\, C_{kj} + \hat{C}_k, \qquad \text{for } k = 1, \ldots, n_{cv} \qquad (2),$$

n_{cv} is the total number of volume occupying components. These components are water, oil, surfactant, and gas, n_p is the number of phases, $\hat{C}_k$ is the adsorbed concentration of species k, and ρ_k is the density of pure component k at a reference phase pressure P_r relative to its density at reference pressure P_{ro}, usually taken at a surface condition of 1 atm.

The phase flux from Darcy's law is given by,

$$\underline{u}_j = - \frac{k_{rj} \underline{\underline{k}}}{\mu_j} \bullet \left(\underline{\nabla} P_j - \gamma_j \underline{\nabla} h\right) \qquad (3),$$

where $\underline{\underline{k}}$ is the intrinsic permeability tensor and h is the vertical coordinate, k_{rj}, μ_j, and γ_j are the relative permeability, viscosity, and specific weight for phase j. The source terms R_k are a combination of all rate terms for a particular component.

Pressure Conservation Equations. The pressure equation is developed by summing the mass balance equations over all volume occupying components, substituting Darcy's law for the phase flux terms, using the definition of capillary pressure, and noting that $(\sum_{k=1}^{n_{cv}} C_{kj}) = 1$. The pressure equation in terms of the reference phase pressure (phase 1) is given by,

$$\phi C_t \frac{\partial P_j}{\partial t} + \underline{\nabla} \bullet \underline{\underline{k}} \bullet \lambda_{rTc} \underline{\nabla} P_j = - \underline{\nabla} \bullet \sum_{j=1}^{n_{cv}} \underline{\underline{k}} \bullet \lambda_{rTc} \underline{\nabla} h +$$

$$+ \underline{\nabla} \bullet \sum_{j=1}^{n_{cv}} \underline{\underline{k}} \lambda_{rTc} \bullet \underline{\nabla} Pc_{jw} + \sum_{j=1}^{n_{cv}} Q_k \qquad (4),$$

where the total relative mobility including the correction for fluid compressibility is given by $\lambda_{rTc} = \sum_{k=1}^{n_{cv}} \lambda_{rjc}$, and $\lambda_{rjc} = \frac{k_{rj}}{\mu_j} \sum_{k=1}^{n_{cv}} r_k C_{kj}$. C_t is the total compressibility calculated as the volume weighted sum of matrix and component compressibilities.

Fluid and Soil Properties. Geological heterogeneities are the key factor that reduces the effectiveness of chemical enhanced recovery processes because their success depends on the delivery of injected chemicals and water into the subsurface. In order to capture some of the geological features, reservoir properties such as formation permeability, porosity, residual phase saturation, phase relative permeability, and phase capillary pressure are allowed to vary spatially in UTCHEM. Phase trapping functions and adsorption of both surfactant and polymer are modeled as a function of permeability.

Polymer Adsorption. Polymer adsorption can be an important mechanism for a chemical recovery project since it causes retardation polymer consumption. The retention of polymer molecules in permeable media is due to both adsorption onto solid surfaces and trapping within small pores. UTCHEM uses a Langmuir-type isotherm to describe the adsorption level of a polymer, which takes into account the salinity, polymer concentration, and soil permeability[8]. The adsorption is irreversible with concentration and reversible with salinity. The adsorbed concentration ($\hat{C}_p$) is given by,

$$\hat{C}_p = \min \{ \tilde{C}_p, \frac{a_p (\tilde{C}_p - \hat{C}_p)}{1 + b_p (\tilde{C}_p - \hat{C}_p)} \} \qquad (5).$$

The minimum is taken to guarantee that the adsorption is no greater than the total polymer concentration. Adsorption increases linearly with effective salinity and decreases as follows,

$$a_p = (a_{p1} + a_{p2} C_{SEP}) k^{-0.5} \qquad (6).$$

The adsorption parameters a_{p1}, a_{p2} and b_p are found by matching laboratory polymer adsorption data. The effective salinity for polymer (C_{SEP}) is,

$$C_{SEP} = \frac{C_{51} + (\beta_p - 1)\, C_{61}}{C_{w1}} \qquad (7),$$

where C_{51}, C_{61}, and C_{w1} are the anion, calcium, and water concentrations in the aqueous phase and β_p is experimentally determined.

Viscosity. Liquid phase viscosities are modeled in terms of pure component viscosities and the phase concentrations of the organic, water and chemicals,

$$\mu_k = C_{wk}\,\mu_k\, e^{\alpha_w (C_{ok} + C_{chk})} + C_{ok}\,\mu_k\, e^{\alpha_o (C_{wk} + C_{chk})} + C_{chk}\,\mu_k\, e^{\alpha_{ch} (C_{wk} + C_{ok})} \qquad (8),$$

for k = water, oil or chemical.

The α parameters are determined by matching laboratory microemulsion viscosities at several compositions. In the absence of polymer, water and oil phase viscosities are reduced to pure water and oil viscosities. When polymer is present μ_w is replaced by μ_p defined below.

The viscosity of the polymer solution depends on the concentration of polymer and on salinity,

$$\mu_p^o = \mu_w \{1 + (A_{pw}\, C_{pw} + A_{po}\, C_{pw}^2 + A_{pch}\, C_{pw}^3)\, C_{SEP}^{Sp} \} \qquad (9),$$

where C_{pw} is the polymer concentration in water, μ_w is the water viscosity, A_{pi} are constants. The factor C_{SEP}^{Sp} allows for dependence of polymer viscosity on salinity and hardness.

The reduction in the viscosity of the polymer solution is a function of shear rate (γ) and is modeled by using Meter's equation[9],

$$\mu_p = \mu_w + (\mu_p^o - \mu_w) / (1 + \{ \gamma / \gamma_{1/2} \}^{P\alpha - 1}) \qquad (10),$$

where $\gamma_{1/2}$ is the shear rate at which viscosity is the average of μ_p^o and μ_w, and P_α is an empirical coefficient.

Surfactant/Brine/Oil phase behavior. The surfactant-oil-water phase can be represented as a function of effective salinity once the binodal curve and the tie-lines are described. The phase behavior model in the UTCHEM simulator uses Hand's rule[10], and is base on the work by Nelson and Pope[6], Satoh[11] and Camilleri et al.[12]. The effective salinity increases with the divalent cations bounded to micelles (Camilleri et. al.[12], Hirasaki[13]) and decreases as the temperature increases for anionic surfactants. Effective salinity concentration (C_{Se}) is calculated using,

$$C_{Se} = \frac{C_{51}}{(1 - \beta_6\, f_6^s)\,[1 + \beta_T (T - T_{ref}]} \qquad (11),$$

where C_{51} is the aqueous phase anion concentration; β_6 is a positive constant; f_6^s is the fraction of the total divalent cations bounded to the surfactant micelles; and β_T is the temperature coefficient.

The formulation of the binodal curve using Hand's rule[10] is assumed to be the same in all phase environments. Hand's rule is based on the empirical observation that equilibrium phase concentration ratios are straight lines on a log-log plot scale. Figures 3a and 3b show a type II(-) ternary diagram and its corresponding Hand plot. The binodal curve is computed from,

$$\frac{C_{3j}}{C_{2j}} = A \left\{ \frac{C_{3j}}{C_{1j}} \right\}^B, \text{ with } j = 1,2, \text{ or } 3 \qquad (12),$$

where A and B are empirical parameters. For a symmetric binodal curve where B = -1 all phase concentrations are calculated explicitly in terms of oil concentration C_{2j}.

$$C_{3j} = 0.5 \left[- A\, C_{2j} + \sqrt{(A\, C_{2j})^2 + 4\, A\, (1 - C_{2j})} \right], \text{ for } j = 1,2, \text{ or } 3 \qquad (13).$$

Parameter A is related to the height of the binodal curve as,

$$A_m = \left\{ \frac{2\, C_{3max,m}}{1 - C_{3max,m}} \right\}, \text{ for } m = 0,1, \text{ and } 2 \qquad (14),$$

where 0, 1, and 2 are numbers related to the maximum heights of the binodal curve measured for low, optimal and high salinities. The height of the binodal curve is specified as a linear function of temperature:

$$C_{3max,m} = H_{BNC,m} + H_{BNT,m} (T - T_{ref}) \qquad (15),$$

where $H_{BNC,m}$ and $H_{BNT,m}$ are input parameters. A_m is linearly interpolated as,

$$A = (A_o - A_1) \left[1 - \frac{C_{Se}}{C_{Seop}} \right] + A_1, \text{ for } C_{Se} \le C_{Seop} \qquad (16),$$

$$A = (A_2 - A_1) \left[\frac{C_{Se}}{C_{Seop}} - 1 \right] + A_1, \text{ for } C_{Se} \ge C_{Seop} \qquad (17),$$

where C_{Seop} is the optimum effective salinity calculated as the arithmetic average of C_{Sel} and C_{Seu}. The heights of the binodal curve at three reference salinities are estimated based on phase behavior laboratory experiments.

EXPERIMENTAL PART

Several chemical systems were tested to determine oil recovery potential for an oil mixture designed with a viscosity of approximately 10 cp. The tests included phase behavior

observations, viscosity measurements, interfacial tension measurements, and a linear oil recovery experiment. The suggested chemical system is composed of a surfactant (petroleum sulfonate), co-surfactant (2-methyl, 1-propanol), and a high molecular weight polyacrylamide polymer.

MATERIALS:

Oil. Two oil mixtures were formulated to obtain a paraffin-based oil with an approximate viscosity of 10 cp at ambient temperature. Oil 1 consisted of 68% motor oil (SAE 30 non detergent motor oil) and 32% decane. Oil 2 was 66.5% Soltrol 220 (isoparaffinic oil from Phillips Petroleum Co) and 33.5% SAE 30 motor oil. The viscosity of Oil 2 is 11.6 cp at 23 °C and 9.88 cp at 30 °C. The viscosity of Oil 1 is 9.32 cp at 30 °C and is slightly higher at ambient temperature (10.9 cp).

Surfactant/Co-surfactant. The co-surfactant used for these studies was 2-methyl, 1-propanol (isobutyl alcohol or IBA). Alcohol molecules are incorporated in surfactant micelles and change surfactant solution properties (such as viscosity, partitioning, and solubility). Two petroleum sulfonate surfactants from Witco Corporation were tested. Table 1 summarizes surfactant information. All surfactant/co-surfactant mixtures were prepared by wt%/wt% in different concentration sodium chloride solutions. The alcohol was always used at the same concentration as the surfactant.

Polymer. The polymer is a high-molecular-weight hydrolyzed polyacrylamide, Alcoflood 1275, from Allied Colloids, which is available in powder form. This polymer is anionic, and its average molecular weight is 22×10^6 dalton.

EQUIPMENT AND PROCEDURES:

Physical Properties. Viscosities were measured with a Brookfield Cone and Plate viscometer. IFTs (interfacial tension measurements) were determined with a spinning drop tensiometer.

Phase behavior of the surfactant/brine/oil system was determined by mixing equal volumes of aqueous and oil phases in tubes made from 10 cc pipets which have had the tips sealed to prevent fluid leaks. Volumes can be read to 0.1 cc from the marking on the pipets. To determine optimal salinity and the 3-phase salinity region, a series of tubes is prepared with different salt concentrations. The tubes are shaken and allowed to equilibrate. If surfactant remains in the aqueous phase after equilibration, the salinity is under optimum and is designated II(-). If the surfactant partitions into the oil phase, salinity is over optimum and is designated II(+). If three phases form (oil, brine, and middle phase), the behavior is designated III.

Oil Recovery. The idea behind the experimental program is to observe experimentally movements of surfactant - oil bank flood fronts in well-characterized cores and a quarter 5-spot model. The displacement in a low heterogeneity core is one-dimensional when appropriate flow rate is used. The results of these experiments provide the mobility of all the fluid banks and help conform the mechanistic model in one-dimension. The floods in a quarter 5-spot model provide experimental data on movement of surfactant-oil bank in multi-dimensions. In some cases, surfactant-oil bank front will be stable and in some

cases, it will be unstable. The effect of surfactant slug composition on movement of this front is studied. The interaction between the polymer mobility buffer and the surfactant slug is studied. The influence of salinity on phase behavior and oil recovery is recorded.

Core Experiments. Oil recovery experiments were conducted in a Berea sandstone core plug 1.5 in. in diameter and 9.5 in. long. Core permeability was 506 md at 100% water saturation. Porosity was 23.3%. The core was initially saturated with non damaging brine, then oil was flooded to residual water saturation, and saturated with water to residual oil saturation before conducting the chemical flood experiment. Figure 4 shows the Hassler sleeve apparatus and experimental equipment used in the oil recovery tests.

Quarter 5 Spot Apparatus. A porous medium was prepared in two different geometries: a cylindrical core and a quarter five-spot. The cylindrical core (2.54 cm diameter, 30.48 cm long) was used to determine the relative permeability of the medium. The quarter five-spot is used to conduct the immiscible floods. The quarter five-spot model consists of a porous medium approximately 41.9 cm x 41.9 cm x 2.54 cm in size. It has a thin plastic plate above the porous medium. This plate is pressurized from above to prevent channeling. The overburden pressure is kept higher than the pressure inside the porous medium. The porous medium consists of a mixture of glass beads of a specified bead radius distribution in the range of 25 to 100 mesh (0.706 - 0.15 mm). There is an injection port at each of the four corners. Two diagonally opposite corners are usually closed during most displacement experiments. Thus the model represents one quarter of the 5-spot patterns used in oil fields. The key properties of the quarter 5 spots model dimensions are listed in Table 3.

A cylindrical packed bed was used to determine relative permeabilities of the fluids used in these experiments. The relative permeability of the cylindrical porous pack is determined by the steady state method. Brine solutions and oil are injected simultaneously at different fractional flows with the total flow rate being constant. At each steady state, the pressure drop is measured by a differential pressure transducer and the saturation is estimated by material balance. Three different saturation histories can be traversed: primary drainage, imbibition and secondary drainage. Primary drainage experiments have been conducted to evaluate the level of homogeneity of the quarter five spot apparatus. Second drainage experiments were not conducted in this research.

Immiscible displacements at adverse viscosity ratios are conducted in a quarter five-spot model in both the drainage and the imbibition modes at comparable viscosity ratios and density differences. The nonwetting fluid is the injectant in the drainage model, whereas the wetting fluid is the injectant in the imbibition mode. The quarter five-spot model is first filled with brine of a given concentration. This fluid is then miscible displaced by a glycerol-water solution of high viscosity. A viscous oil is then injected to displace the water and drive the model to its residual water saturation. Then a colored low viscosity brine solution of a suitable concentration is injected to displace the viscous oil. The fingering in this adverse viscosity, immiscible, imbibition flow is then visualized. The injection rate was 1 ml/min. in these displacements. The fluids used and their properties are listed in Table 4. The effluent composition and the pressure drop were monitored. Photographs can be taken from the top and sides of the model during experiments.

The viscosity ratio (μ_o/μ_b), the ratio of the viscous to gravity forces, and the ratio of the field-scale capillarity to viscous forces are approximately honored in this model for typical field applications. The capillary number (10^{-7} - 10^{-5}) is, however, not honored. The effluent is analyzed for oil, solvent and water production. After finishing one displacement experiment the model is resaturated with oil to prepare the model for next flood.

The oil recovery experiments involve, surfactant slug, 0.20 PV in size, polymer slug at a fixed brine concentration, 0.80 PV in size and brine flooding, without polymer up to 4 PV of total injected fluids. Three different salinity concentrations, below, above and at the optimal salinity were used. Some salinity gradient experiments adding a second polymer slug at a lower brine concentration (0.9%) than the primary mobility buffer (1.4%) were also conducted. This second polymer slug was 1 PV in size. No preflushes were conducted in these experiments.

RESULTS

PHASE BEHAVIOR AND INTERFACIAL TENSION

A quick screen test using Oil 1 and Witco EOR 2094 Surfactant to determine salinity effect on 3-phase formation indicated that a middle phase would form around the 1% NaCl concentration region. Very low IFT values were measured between this oil and surfactant in 1% NaCl, as shown in table 2.

In the case of Oil 2 and Witco EOR 2095 a phase tubes experiment showed 3-phase behavior for salinities between 1.1 and 1.45% NaCl. Figure 5 shows the phase volumes, and Figure 6 shows the solubilization parameters for this system. Optimum salinity was approximately 1.39% NaCl. The presence of polymer in the solution did not change the optimum salinity. The optimum salinity changed slightly as the ratio of oil components changed. An oil mixture of 87.5% Soltrol 220 and 12.5% motor oil had an optimum salinity of 1.22%. Optimum salinity also decreased as the concentration of surfactant decreased. A 1% surfactant solution with Oil 2 showed a 3-phase region from 0.75% NaCl through 1.2% NaCl. A 0.5% surfactant solution produced a small third phase around 1% salinity. IFT values between Oil 2 and 3% EOR 2095 at optimum salinity were not as low as the IFTs between Oil 1 and 3% EOR 2094.

It was found that Alcoflood 1275 polymer develops the highest viscosity in low salinity brine. Adequate viscosity is generated, however, by a 1,000 ppm polymer solution when prepared in a sodium chloride solution at optimal salinity for the surfactant/oil mixtures under study.

OIL RECOVERY

Core Experiments. Oil recovery in a linear flow configuration was conducted using the following fluids:

- Brine 1.4% NaCl

- Oil — 66.5% Soltrol 220, 33.5% non detergent motor oil SAE 30
- Surfactant — 3% Witco EOR 2095, 3% 2-methyl, 1-propanol in 1.39% NaCl, and 1,000 ppm 1275 polyacrylamide.
- Polymer — 1,000 ppm Alcoflood 1275 polyacrylamide in 1.4% NaCl
- Chase brine — 1.4% NaCl

The planned chemical injection volumes were 0.2 PV or less of surfactant and 1.0 PV or less of polymer. Actual injected PVs were 0.20 for surfactant and 0.77 for polymer. The fluids were injected at a rate of 10 ft/day. Note that this is not a salinity gradient experiment. The system, however, produced over 90% of the oil remaining after waterflood as shown in Figure 7. Some emulsions were produced toward the end of the oil production. They were broken by addition of a small amount of 2-propanol (IPA). These results indicate that the chemical system appears to have adequate oil recovery capabilities.

Quarter 5-Spot Experiments. Figure 8 shows the steady state relative permeabilities measured in a linear core for imbibition experiments. The residual water saturation at the beginning of the imbibition flood is approximately 8 %. The residual oil saturation at the end of the imbibition run is approximately 17 %. The water relative permeability showed little hysteresis between primary drainage and imbibition. The oil relative permeability at residual water saturation is 0.49, typical of bead beds, significantly lower than 1 (which is typical of water-wet sandstones). The water relative permeability at residual oil saturation is about 0.51.

The immiscible drainage and imbibition displacements conducted on the quarter five-spot model are listed in Table 4. The model was initially 100 % saturated with water. Before the primary drainage, water is displaced by a mixture of water-glycerol. This is a stable displacement because the water-glycerol mixture is more viscous than pure water. Photographs taken during the experiment showed an almost circular displacement front. This circular front indicates that the medium is not very heterogeneous. This model is not homogeneous, but it is not very heterogeneous either, as indicated by the fronts of the stable displacements[14]. As the floods become unstable, heterogeneities become important. Current theory can not describe immiscible viscous fingering in such mildly heterogeneous media adequately. The main problem is to select adequate values for relative permeability. For imbibition floods, it is expected that the pore-scale flow to be stable and independent of capillary number for $N_C < 10^{-5}$. The steady state relative permeabilities should then be applicable to the imbibition floods[15].

Three kind of experiments have been completed at this time, water floods, chemical floods at optimal salinity, and chemical floods at upper salinity. In the case of water floods the following behavior was observed. Macroscopic (1 cm) and microscopic fingers (1 mm) were present during the imbibition and drainage experiments. The viscosity ratio (10.9) in the imbibition run is adverse while the fluids densities are about the same. Six fingers were observed in this flow. Fingers are rounded, compact and follow the bulk flow direction. Drainage experiments using this model showed long and slim fingers. More

microscopic fingers were also observed in the unstable drainage experiments than in the imbibition ones. The bottom of the model is flooded along with the top in the imbibition experiment while it was not flooded at all for more than 1 PV for the drainage experiments. The injectant and the displaced fluids have about the same density, therefore, no significant gravity override was observed.

During the optimal salinity experiments no fingering was observed until after 1 PV injection anywhere in the model. Microscopic fingering started at that time in the middle area of the model. The fingering moved close to the production port later. The onset of macroscopic fingering was observed at about 2 PV. The fingering was also restricted to the upper right corner of the model. This area is close to the production port. No significant fingering was observed elsewhere in the model. Reverse mobility gradient between the chase water and the mobility buffer seems to be the cause of this behavior.

The upper salinity experiments showed microscopic fingering appearing after injection of 0.8 PV. Macroscopic fingering was observed after 1.5 PV injection. The fingers were somewhat thinner than in the optimal salinity case and they also appeared in the right upper corner of the model. They appeared to channel the driving fluid toward the injection port through the displaced fluid. They occupied a somewhat bigger area of the model than in the optimal salinity case. Interpretation of these results is done jointly with the simulation results in the discussion section.

Figure 9 shows the recovery curves for all the experimental floods conducted so far. The recovery for the chemical floods was significantly higher than the recovery for the water flood case.

SIMULATION RESULTS

The UTCHEM simulator has several interesting features that can be used to thoroughly study the chemical flooding process. Saturation, concentration, viscosity, IFT and other property profiles can be obtained as results of appropriate simulation runs. The integration domain is divided in blocks. We used eleven blocks in the x direction in our coreflood studies. The simulator also calculates the system phase behavior block by block, reporting a phase behavior profile that can be compared with the phase behavior information obtained using other properties.

Core Flood Simulations. Typical results for our simulations are shown in Fig. 10. Effective salinity is plotted versus the core axial dimension (x). The effective salinity concentration profile decreases monotonically from the core entrance to the core exit. The first four blocks have an effective salinity concentration higher than the upper limit, therefore, a II(+) behavior is expected for these blocks. A micro-emulsion phase will be at equilibrium with an aqueous phase. Blocks 5 to 8 are within the upper and lower effective salinity limits, therefore, three phases will be at equilibrium in those blocks. Block 5 has been reported to behave as a type 4 phase behavior. According to the UTCHEM simulator convention, type 4 represents the equilibrium in the left lobe (II(+)) of a type III region. Blocks 9 to 11 are located below the lower salinity limit, therefore, a II(-)

behavior is expected for these blocks. A micro-emulsion phase will be at equilibrium with an oil rich phase.

Figs. 11 through 13 show the variation of different properties along the core plug. The variation of these properties can be interpreted using the phase behavior discussed above. The relationship between these properties and the oil recovery efficiency can also be determined from the study of these figures. A zero value for any property in any of the three phases means that this phase is not present in the block under consideration.

Fig. 11 shows the variation of viscosity with position. Oil viscosity is zero for the first four blocks and aqueous phase viscosity is zero for the last three. This result is in agreement with the phase behavior discussed above. The viscosity plays a big role in the efficiency of the recovery process. The aqueous phase is more than ten times less viscous than the oil phase (1 cp to 10.9 cp). Therefore, polymer is added to the mobility buffer to avoid fingering. This figure reflects the situation after injection of 0.5 PV. The viscosity of the aqueous and micro-emulsion phases is higher than the oil phase viscosity for blocks 1 to 7. Blocks 8-11 present higher oil phase viscosity. Other simulation results ,not presented here, showed that the oil bank moves towards the production part of the core as the injected volume increases. In conclusion; the oil bank is pushed towards the production well by the more viscous aqueous and micro-emulsion phases. This situation can be observed in Fig. 12. The oil saturation is zero or nearly zero for the first five blocks and increases very rapidly for the blocks 6 to 11. The micro-emulsion phase saturation profile presents a maximum at block 6 decreasing for blocks 7 to 11. Aqueous phase saturation decreases from blocks 1 to 7. Water is being trapped into the micro-emulsion phase. Then, it disappears in blocks 8 to 11.

Fig. 13 shows values of interfacial tension (IFT) within the core plug. Decimal logarithm of IFT is plotted vs. X direction. There are two possible interfaces for this system micro-emulsion/water and micro-emulsion/oil. The IFT value is different for both interfaces when three phases are present, blocks 6 to 8. Equal IFT values imply than only two phases are present, blocks 1 to 5 and 9 to 11. The figure also shows that from block 1 to 10 the IFT is significant smaller than the pure water IFT value (+1.65 mN/m). These low values are produced because the effective salinity is everywhere within close proximity of the optimal salinity range. This figure is an extreme example of the reduction in IFT reached through adjustment of the effective salinity. The high recovery achieved in this case, even for a high viscous oil, shows the potential of chemical flooding methods to recover residual oil.

Figure 14 shows a comparison between experimental data and simulation results for oil production. There is good agreement for all values between simulation results and experimental data. The biggest discrepancy occurs for small values of PV. The calculated results predict higher recovery than the experimental data. For medium and high volumes the results are practically the same. This figure shows that the simulation results can be used with reasonable confidence to design these processes.

Quarter 5-Spot Results. Typical results for our simulations are shown in Fig. 15. This figure corresponds to an optimal salinity chemical flood after 1.1 PV injection. The

contour plot shows number of phases present, for example, a three value represents; aqueous, oil and micro-emulsion phases present. We can observe that there are three phases present almost everywhere inside the physical model. This phase behavior occurs because the effective salinity is within optimal value range in the whole model. Fig. 16 shows this to be the case. Only at the injection port and small regions on the top and upper right sides of the model are below optimal salinity concentration. Therefore, we can expect these two areas to present two phase behavior instead of three.

Figures 17 to 20 show contour plots of significant properties inside the physical model. Figures 17 and 19 show the saturation profiles for the aqueous and oil phases. The oscillations in values for the aqueous phase saturation seems to be related to phase behavior and not to fingering. Only microscopic fingering was observed in the area close to the injection port, therefore, the difference in saturation values was not caused by flow behavior. Small salinity differences can cause differences in phase behavior, especially composition, therefore, is our opinion that composition differences created the irregular saturation profile shown in Fig. 17. A similar micro-emulsion saturation contour plot, not shown here, showed the same behavior. It should be considered that even when in many cases there was not actual fingering, the presence of diffuse (not clear) interfacial edges was observed. This fuzzy interfaces may suggest the presence of micro-emulsion phases.

Figure 18 shows a water phase viscosity contour plot. An annular front describes the position of the mobility buffer. The leading edge of this front extends from Y=0.8 to X=0.8. The rear part of this front extends from Y=0.6 to X=0.6. No fingering was observed on the leading edge of the front, but microscopic fingering was present in the rear edge. The fingering increased in size and moved towards the production port as the experiment continued. Figure 18 also shows that the location of the mobility buffer corresponds with a region of high viscosity driving a lower viscosity bank in front. The viscosity decreases for the chase water bank moving after the mobility buffer. The presence of this lower viscosity bank can cause a reverse mobility displacement and produce the fingering.

Figure 19 shows that in about 40% of the physical model the oil phase saturation is below the residual oil saturation for the water flood (0.17). The average oil saturation for the whole model at that point is 0.177, very close to the residual oil saturation value. This fact shows that the surfactant presence increases the oil solubility below residual oil saturation, and, therefore, increases oil recovery. Figure 20 shows that the presence of three phases is related to very low interfacial tension values. The presence of three phases creates two interfaces, micro-emulsion/water and micro-emulsion/oil. Typical values for the micro-emulsion/water interface are shown in Fig. 20. Interfacial tension values range from 10^{-4} to 10^{-2} mN/m, -4 to -2 for $\log_{10}$ values; within the physical model. Only areas close to the injection and production ports present higher interfacial tensions. Slightly lower values were computed for the micro-emulsion/oil interface.

A comparison between simulation results and experimental values for the water flood is shown in Fig. 21. The simulation results are significantly higher than the experimental data. The presence of fingering seems to be the cause for the discrepancy. The simulation results did not show any fingering at all. The UTCHEM simulator did not show fingering

for reverse mobility flows without the presence of some "physical heterogeneity" such as, permeability variations . There was much better agreement between the computed results and experimental data for the chemical flows. The fact that there was much less fingering in the other flows seems to be the reason for this improved agreement.

Figure 22 shows the computed recovery results for all the floods. Three different chemicals floods were simulated, upper and optimal salinity and a salinity gradient flood. The salinity gradient experiment produced the highest recovery. The optimal and upper salinity floods followed closely. All chemicals floods increased significantly the recovery compared to the water flood. There was not preflush in all the simulations. The main difference between the salinity gradient and the other chemical floods is the sudden reduction of salinity concentration in the chase water. These results agree well with the experimental data reported by Chou and Shah[3].

The main mechanisms increasing oil recovery in surfactant-polymer flooding are, increased solubility produced by low interfacial tension and improved mobility control. In order to understand how both mechanisms affect recovery in our floods we plotted average phase saturations vs. PV injected for the optimal salinity and the salinity gradient floods. Figures 23 and 24 show our results. Fig. 23 shows that the oil phase saturation decreases during the flood, reaching a practically constant value (0.17) after 1.5 PV. The aqueous phase saturation increases continuously during the calculation. The micro-emulsion phase average saturation presents a maximum at 0.5 and then decreases in value. The final average saturation value for the micro-emulsion phase is 0.11. The total recovery for this flood is 76%. A volume balance for the oil phase accounts only for 93% of the oil volume originally in place, 76% produced and 17% retained as residual oil saturation. The other 7% was found to be dissolved in the micro-emulsion phase. If the final average saturation value for this phase is 11% we can conclude that the micro-emulsion phase is an "oil-rich" phase. This conclusion shows that the very low interfacial tension does indeed solubilized the oil. Unfortunately, a contour plot of micro-emulsion phase viscosity after 4 PV shows that the micro-emulsion phase has very high viscosity in the region close to the production port. Most of the micro-emulsion phase is located in this region after 4 PV injected. This viscosity is higher than the chase water viscosity and produces channeling and fingering in the region close to the production port. An analysis of the composition of the micro-emulsion phase shows that the high viscosity is produced by polymer solubility in this phase. The practical implication of these findings is that despite the fact that you solubilized a big amount of oil you can not produced part of it. The micro-emulsion phase is trapped in the regions close to the production port and can not be mobilized due to the reverse mobility gradient. In this simulation 7% of the total oil in place is trapped under these conditions.

Fig. 24 shows a similar plot for the salinity gradient case. The oil phase behaves similarly to the previous case, reaching a practically constant value (0.19) after 1.5 PV. The behavior of the system is the same up to 1.1 PV injected. This ,of course, is expected, but a completely different behavior occurs after this PV value. The salinity shock decreases the salinity concentration from 1.4% to 0.9%. The change in salinity changes drastically the phase behavior with an increasing area of the physical model where only two phases are present. The phase behavior is II(-), i.e., you have a micro-emulsion phase and an oil

phase. The salinity shock produces a second maximum in the micro-emulsion phase average concentration. This increase is produced at the expense of the aqueous phase that decreases up to a very low value (0.06). There is a recovery of the relative average saturation values of the aqueous and micro-emulsion phase as the simulation proceeds, though. The micro-emulsion phase continuously decreases after 1.5 PV and the aqueous phase continuously decreases. The final average saturation value for the micro-emulsion phase is 0.255. This final value is significantly higher than the final value in the optimal salinity simulation (0.11). A viscosity contour plot also shows that this micro-emulsion phase presents high viscosity. The reason is also polymer solubility in this phase. Therefore, the micro-emulsion phase is also trapped in the region close to production port as was the case in the previous experiment. An analysis of the concentration of this micro-emulsion phase shows that only 3% oil is retained in this case. The main difference between both cases seems to be that the optimal salinity slug solubilizes more oil than the lower salinity slug produced during the salinity gradient flood. The total oil production in this case, 78.8%, was the highest of all the floods. The conclusion in this case is that despite the fact that less oil is solubilized more of it can be produced. The reason is that the polymer solubility increases at lower salinity concentration[3] and, therefore, better mobility control exists.

This interplay between phase behavior and mobility control should be optimized to improve oil recovery by chemical methods.

CONCLUSIONS

Fluid systems were evaluated for oil recovery studies in this project. The selected chemicals and fluids allow adjustments in fluid properties to study surfactant-polymer interactions under variable but controlled conditions. These properties were successfully tested in linear and quarter 5-spot flooding experiments. Simulation results agreed satisfactorily with experimental data for linear and quarter 5-spot floods. Simulation results allowed us a thorough evaluation of the properties affecting recovery efficiency. Phase behavior was determined primarily by the effective salinity value. A flooding experiment conducted within a small range of optimal salinity can achieve very low IFT and increased "solubility" of the oil in a micro-emulsion phase. Mobility control was also important. The presence of a mobility buffer with a viscosity equal or higher than the mobilized oil increased significantly the recovery efficiency. The interaction between increased solubility and mobility control seems to determine the success of the recovery. In conclusion these experiments and calculations showed the potential of micellar-polymer flooding as a tertiary oil recovery process.

REFERENCES

1. Lake, L. W. "Enhanced Oil Recovery," *Prentice Hall*, New Jersey, 1989.
2. Holm, , L. W. "Effect of Oil Composition on Miscible-Type Displacement by Carbon Dioxide," *Society of Petroleum Engineering Journal*, **22**, 87-98(1982).
3. Chou, S. I. and Shah, D. O. "Optimal Salinity of Polymer Solution in Surfactant-Polymer Flooding Processes," in Surface Phenomena in Enhanced Oil Recovery, edited by D. O. Shah, Plenum Press, New York and London, 1981.
4. Hirasaki, G. J., van Domselaar, H. R. and Nelson, R. C. "Evaluation of the Salinity Gradient Concept in Surfactant Flooding," *Society of Petroleum Engineering Journal*, **23**, 486-500(1983).
5. Pope, G. A., Ben Wang. and Kerming Tsaur, F. G. "A Sensitivity Study of Micellar-Polymer Flooding," *Society of Petroleum Engineering Journal*, **19**, 357-358(1979).
6. Nelson, R. C. and Pope G. A. "Phase Relationships in Chemical Flooding," *Society of Petroleum Engineering Journal*, **18**, 325-338(1978).
7. Reed, R. L. and Healy, R. N. "Some Physico-Chemical Aspects of Microemulsion Flooding: A Review," Improved Oil Recovery by Surfactant and Polymer Flooding, D. O. Shah and R. S. Schecter editors, Academic Press, New York, 1977.
8. Pope G. A. and Nelson R. C., "A Chemical Flooding Compositional Simulator," *Society of Petroleum Engineering Journal*, **18**, 339-354(1978).
9. Meter, D. M., Bird, R. B., "Tube Flow of Non-Newtonian Polymer Solutions, Parts I and II- Laminar Flow and Rheological Models," AICHE J., 878-881 and 1143-1150, (1964).
10. Hand, D. B. "Dineric Distribution: I. The Distribution of a Consolute Liquid Between Two Immiscible Liquids," J. of Physics and Chem., **34**,1961-2000(1939).
11. Satoh, T. "Treatment of Phase Behavior and Associated Properties Used in a Micellar-Polymer Flooding Simulator," M. S. Thesis, The University of Texas at Austin, Aug. 1984.
12. Camilleri, D., Fil., A., Pope G. A. and Sepehrnoori, K., "Improvements in Physical Property Models Used in Micellar-Polymer Flooding," *SPE Reservoir Engineering*, Nov. 1987.
13. Hirasaki, G. J. "Application of the Theory of Multicomponent, Multiphase Displacement to Three-Component, Two-Phase Surfactant Flooding," *Society of Petroleum Engineering Journal*, **21**, 191-204(1981).
14. Stokes, J. P. at al. "Interfacial Stability of Immiscible Displacement in a Porous Medium," *Phys. Rev. Letters,* (1986), 1718-1721.
15. Pavone, D. "Observations and Correlations for Immiscible Viscous Fingering Experiments," *SPERE* (1992) 10(5), 187-194.

TABLES AND FIGURES

TABLE 1. Petroleum Sulfonates from Witco Corporation		
	EOR 2094	EOR 2095
	Petroleum Sulfonate	Petroleum Sulfonate
Equivalent Wt.	422	416
% Active	50.6	50

Table 2. IFT as a function of time for Oil 1 and EOR 2094	
3% 2094, 3% IBA, 1.0% NaCl	
SAE 30/32% Decane	**IFT (mN/m)**
Time (min.)	0.00565
0	0.00458
2	0.00559
5	0.00560
10	0.00582
15	0.00323
25	0.00341
	0.00326

Table 3. Quarter 5-Spot Characteristics	
Thickness (m)	0.0254
Width (m)	0.419
Area (cm^2)	1755.6
Pore Volume (ml)	1627.6
Porosity	0.365
Permeability (darcys)	15

Table 4. Immiscibles Displacements.		
Displacement	Drainage	Imbibition
Displacing fluid ρ (g/cc) μ (cp)	Oil 0.89 10.9	Water 1.01 1
Displaced fluid ρ (g/cc) μ (cp)	Water 2 1.21 10.1	Oil 0.89 10.9
$\Delta\rho$ (gm/cc)	0.21	-0.42
Viscosity ratio	10.1	1.08
Initial S_w	1	0.08

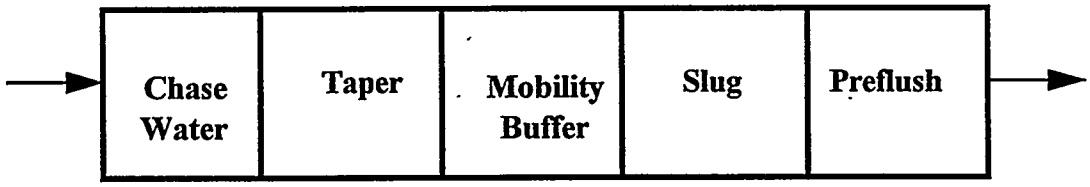

Mobility Buffer
250-2500 g/m3 polymer
0-1% alcohol
Stabilizers
Biocide
0-100%PV

Slug
1-20% Surfactant
0-5% Cosurfactant
0-5% Alcohol
Polymer
5-20%PV

Preflush
Electrolyte (Na, Ca, etc.)
Sacrificial Chemicals
0-100%PV

Fig. 1. Cross section of a typical micellar-polymer flood.

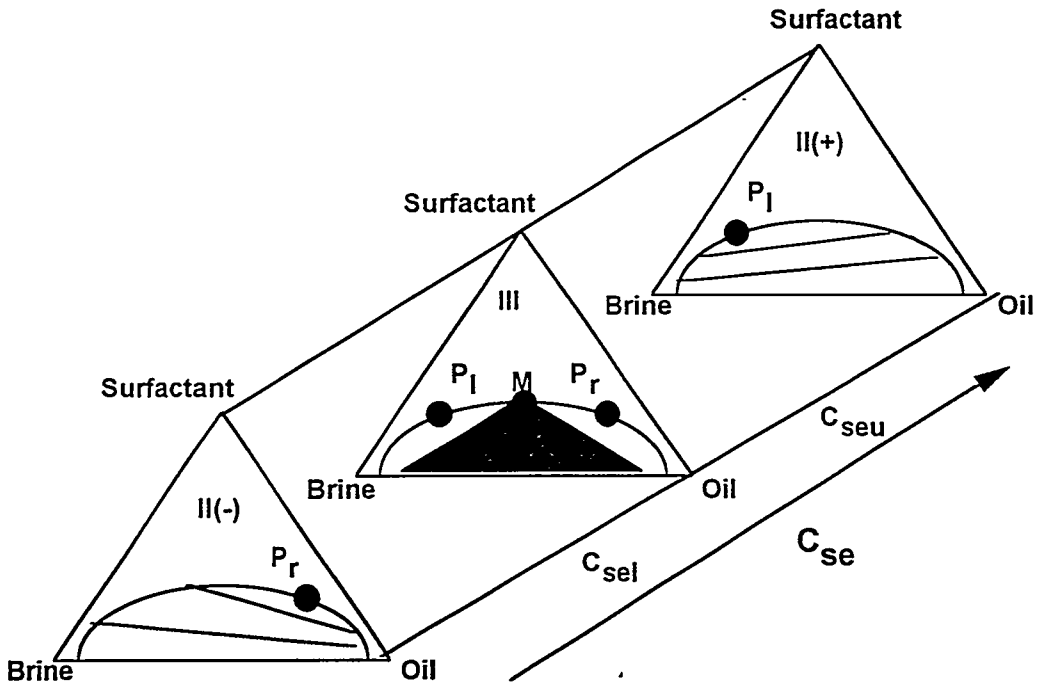

Fig. 2. Ternary diagram representation of micellar-polymer phase behavior.

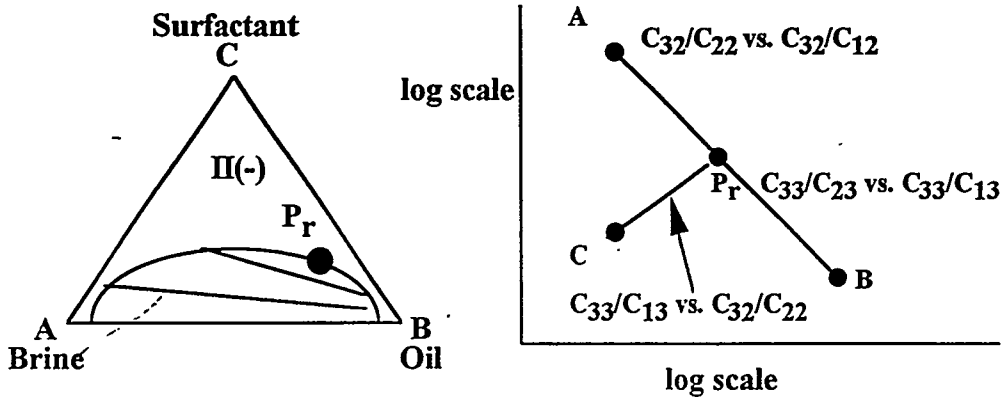

Fig. 3. Correspondence between a ternary diagram and a Hand plot.

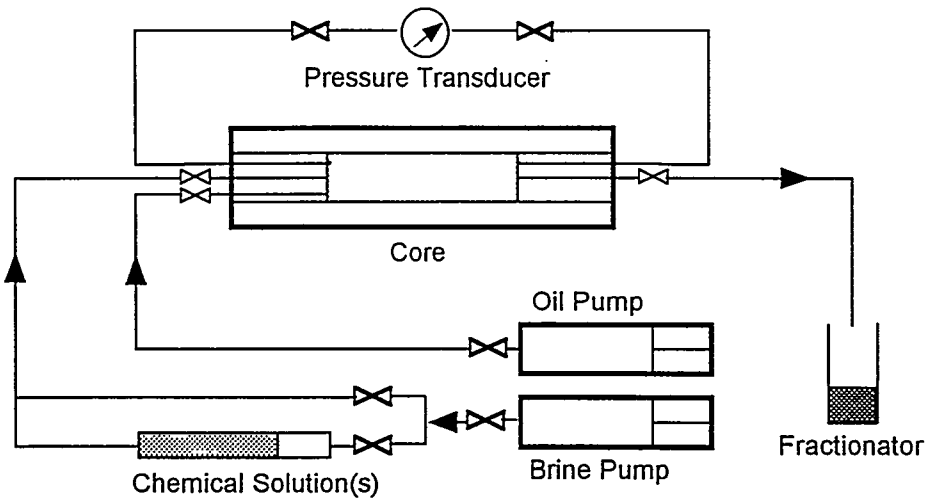

Fig. 4. Core flood apparatus

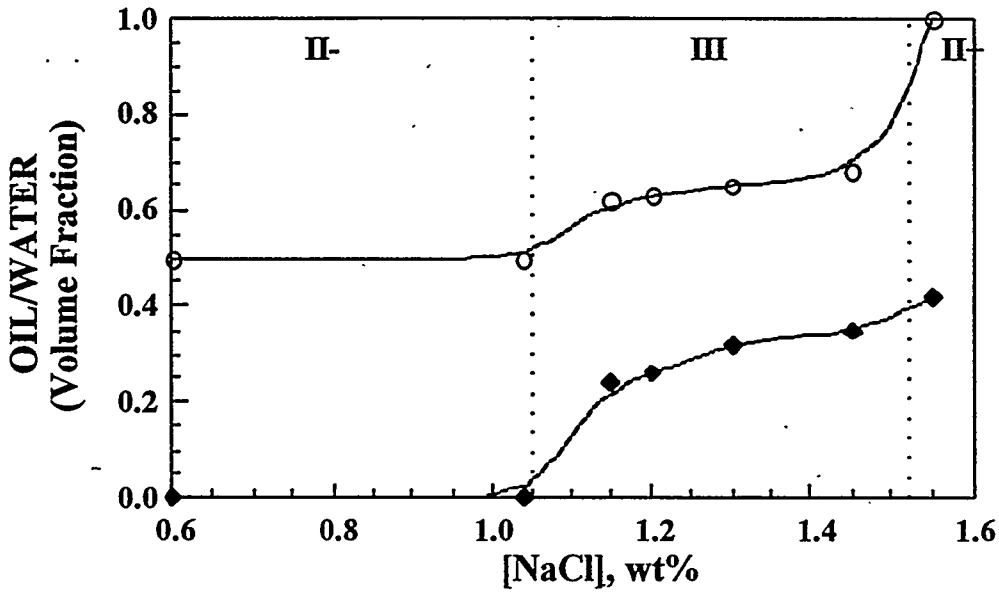

Fig. 5. 2-phase and 3-phase regions as a function of increasing salt concentration for the Witco EOR 2095 surfactant and Oil 2.

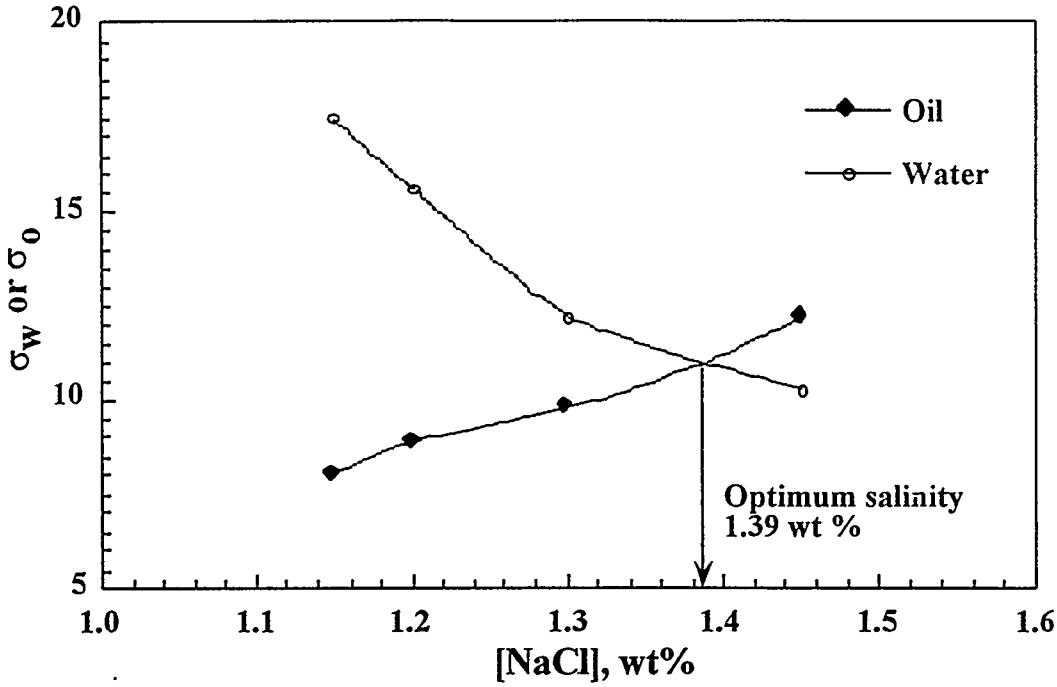

Fig. 6. Oil and water solubilization parameters as a function of salinity. Optimum salinity for the system is at a concentration of approximately 1.39% NaCl.

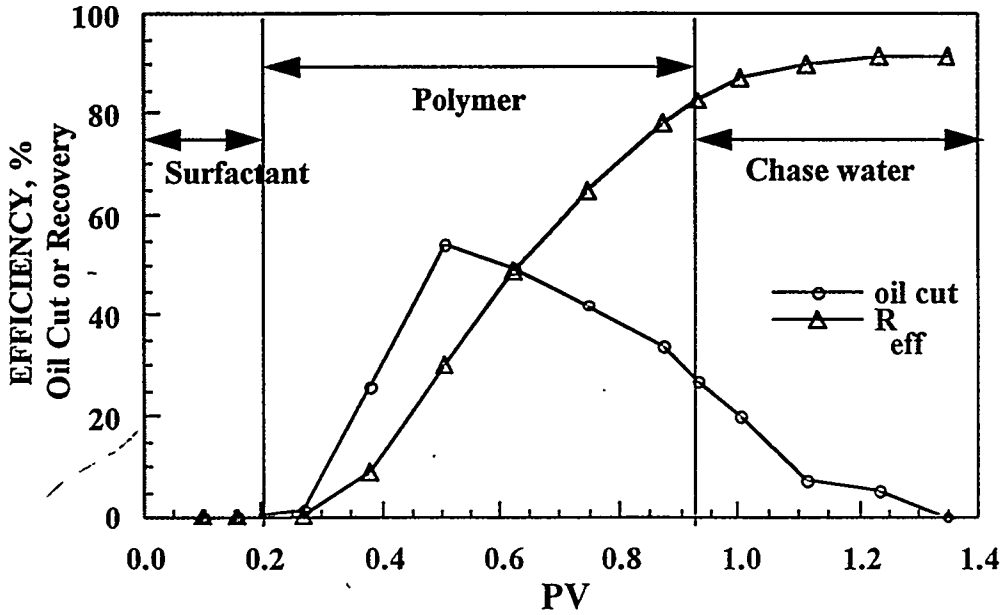

Fig. 7. Oil cut and recovery efficiency as a function of fluid injected for an oil recovery experiment in a Berea sandstone core plug.

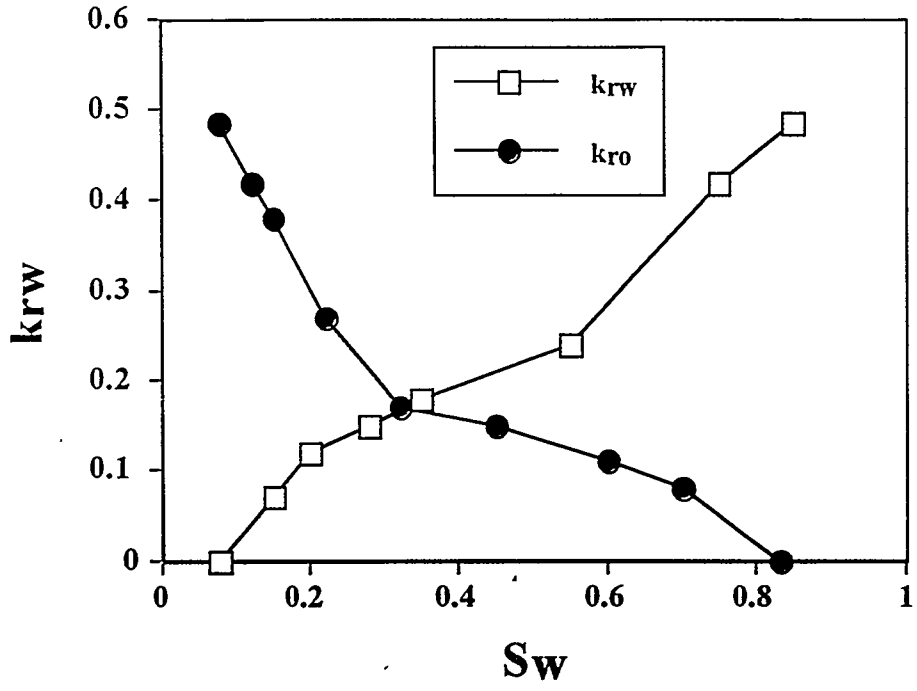

Fig. 8. Steady-state relative permeabilities for imbibition experiments.

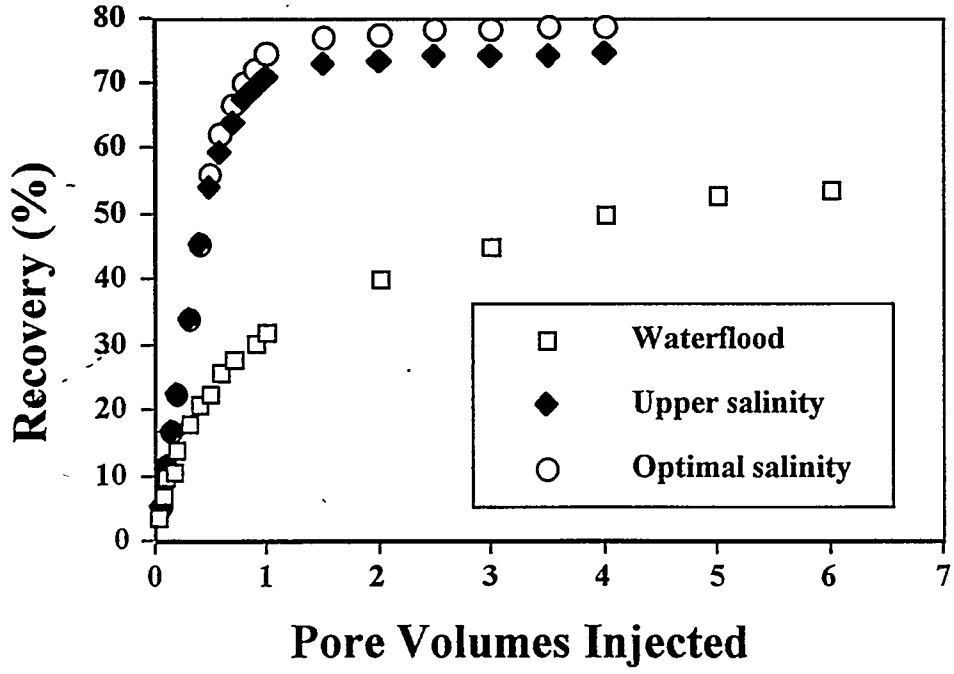

Fig. 9. Experimental recovery curves.

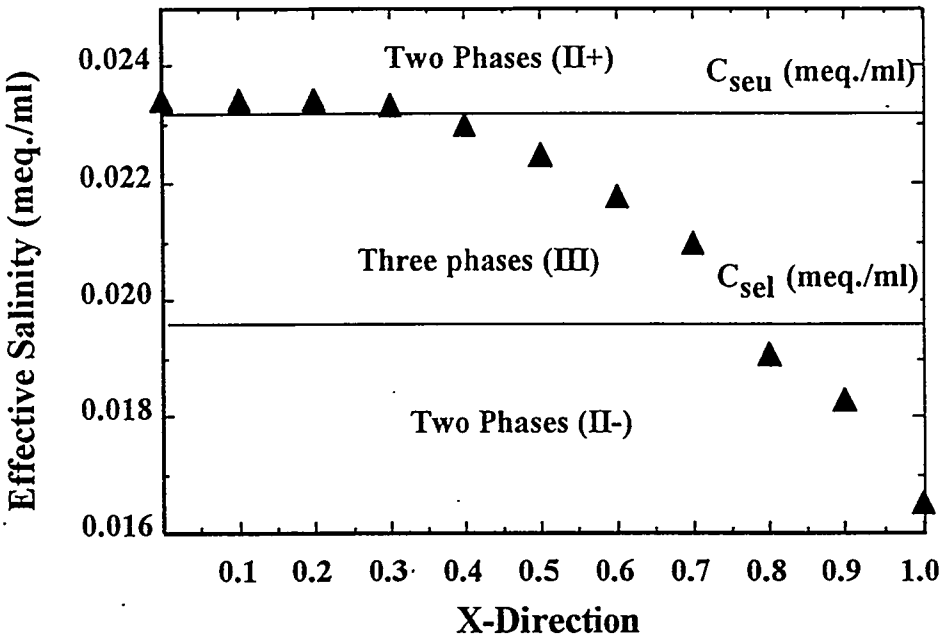

Fig. 10. Relationship between phase behavior and effective salinity along the Berea core plug.

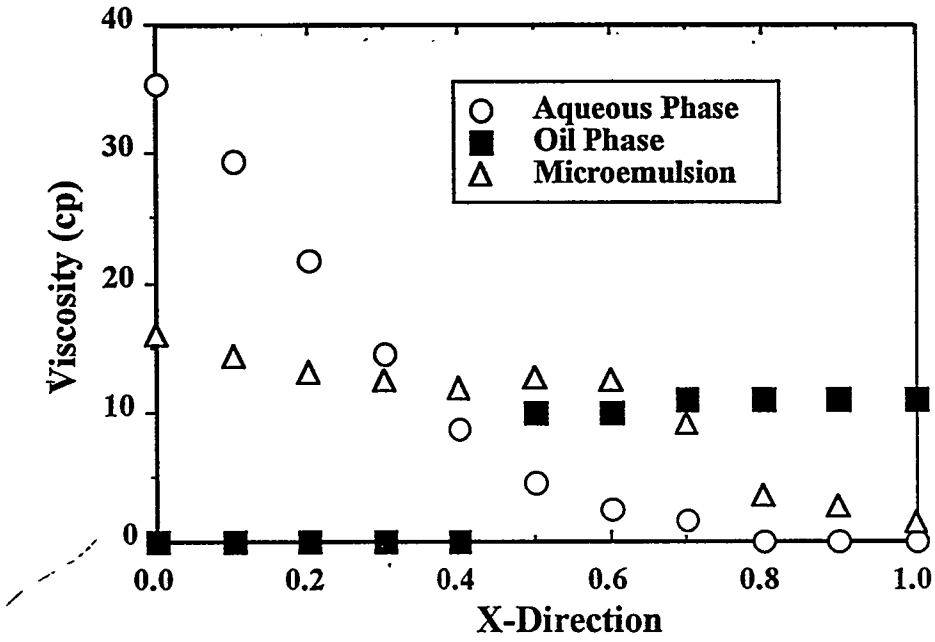

Fig. 11. Viscosity change along the Berea core plug.

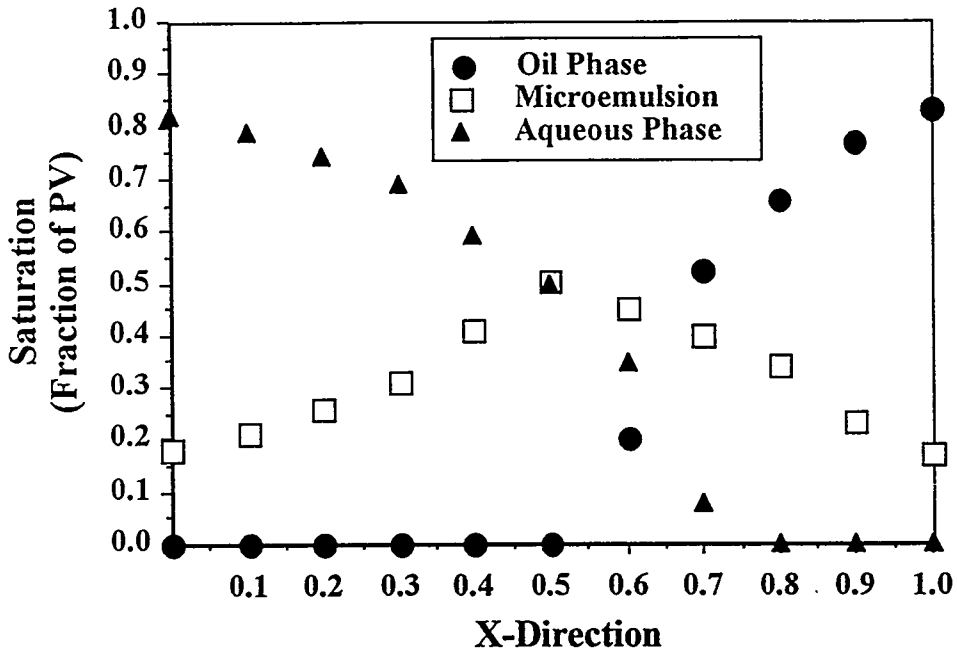

Fig. 12. Phase saturations inside the Berea core plug.

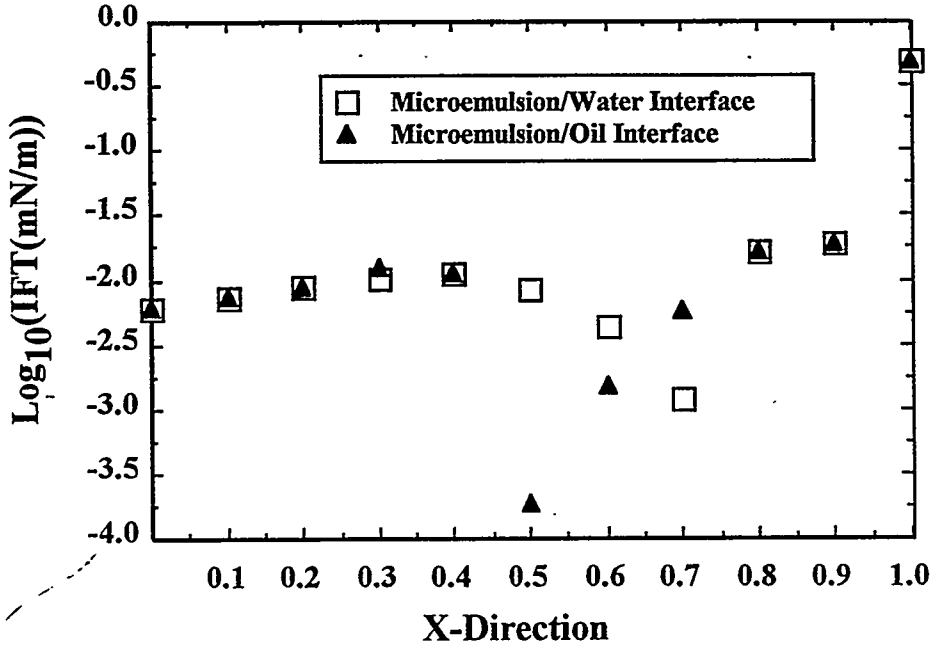

Fig. 13. Interfacial tension (IFT) along the Berea core plug.

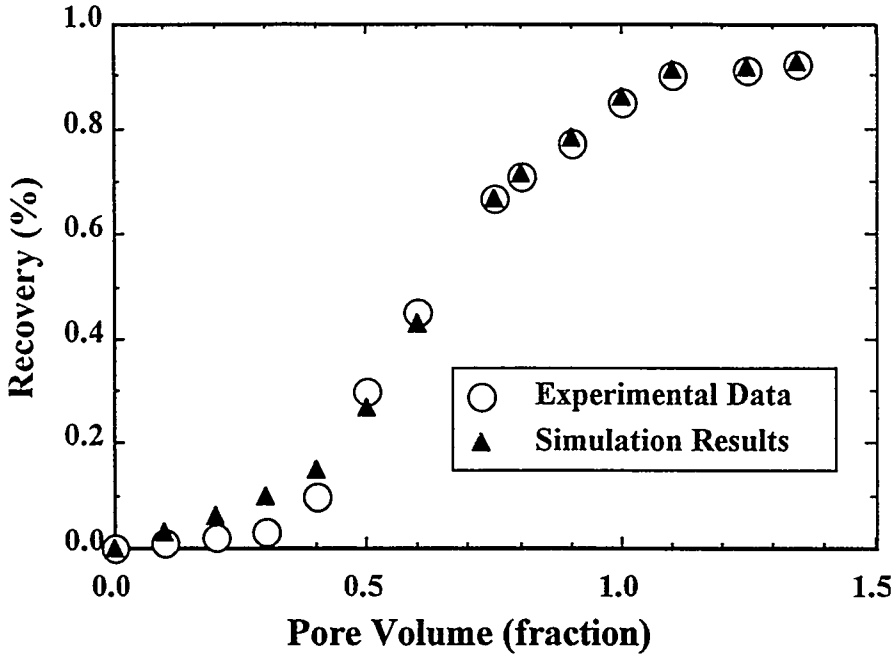

Fig. 14. Comparison of experimental data and simulation results for linear displacements.

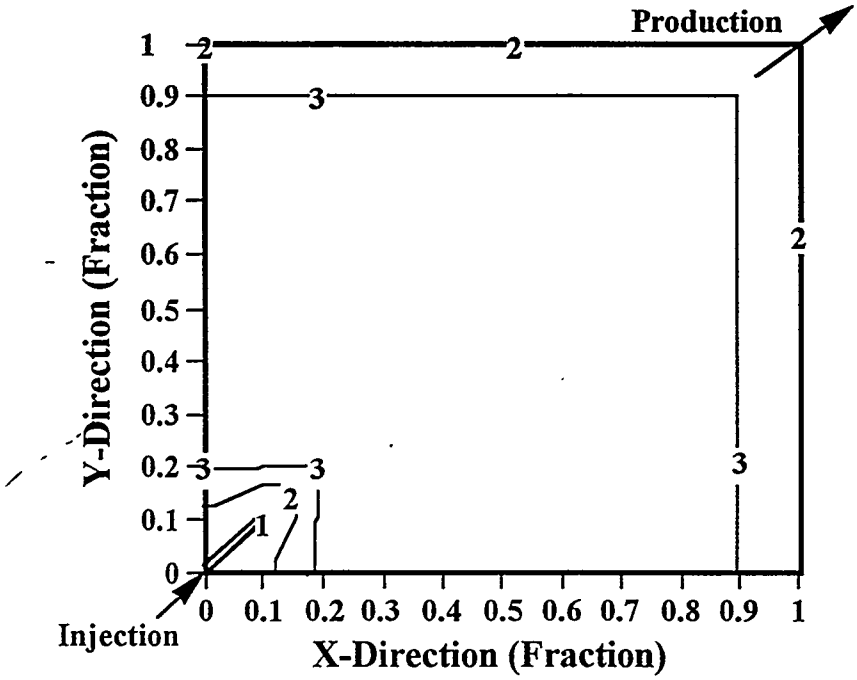

Fig. 15. Phase behavior after 1.1 PVs injected.

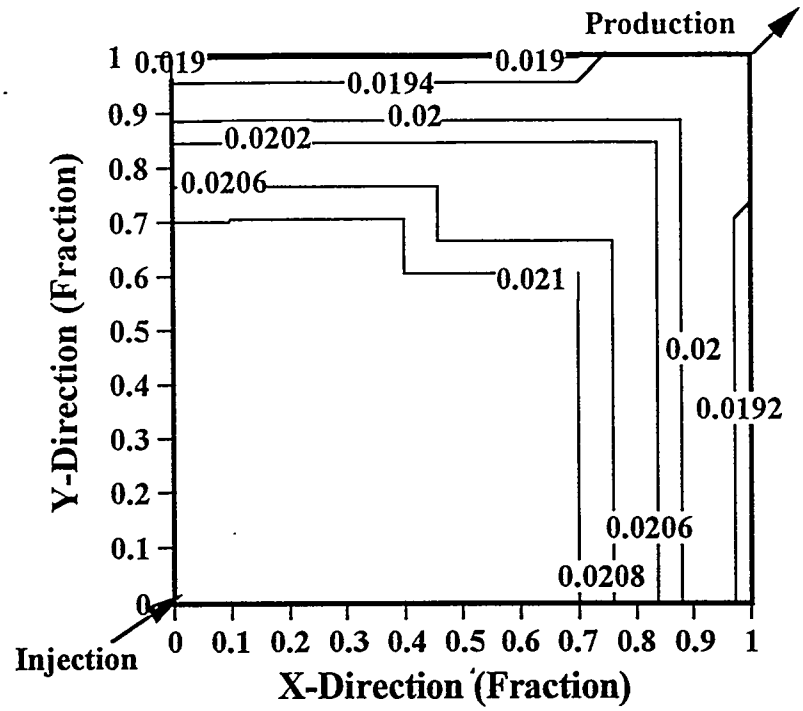

Fig. 16. Effective salinity (meq./ml) contour after 1.1 PVs injected. Optimal salinity between 0.0198 and 0.023 meq./ml.

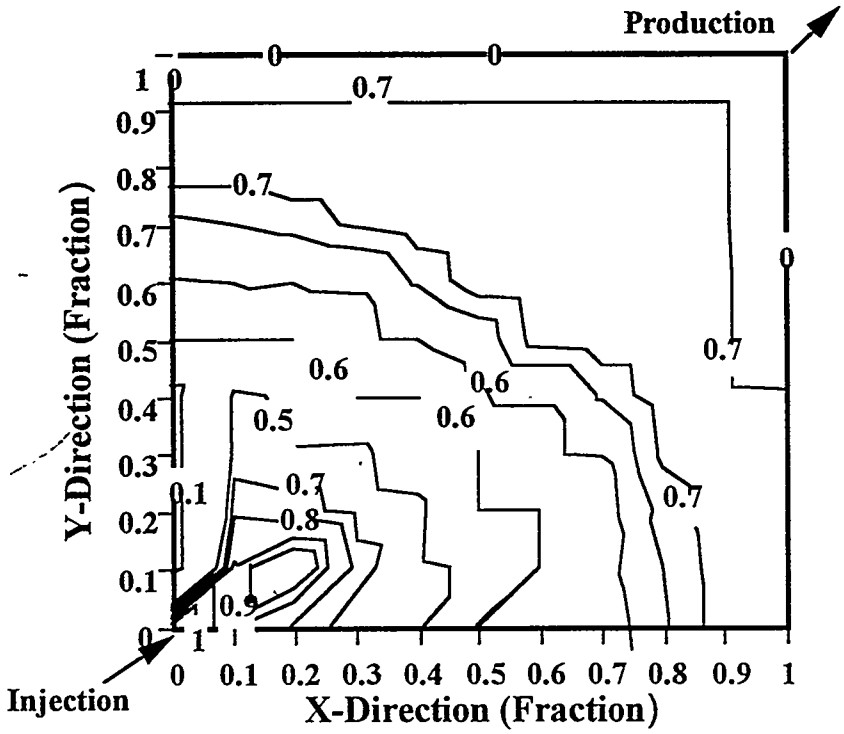

Fig. 17. Water saturation contour after 1.1 PVs injected.

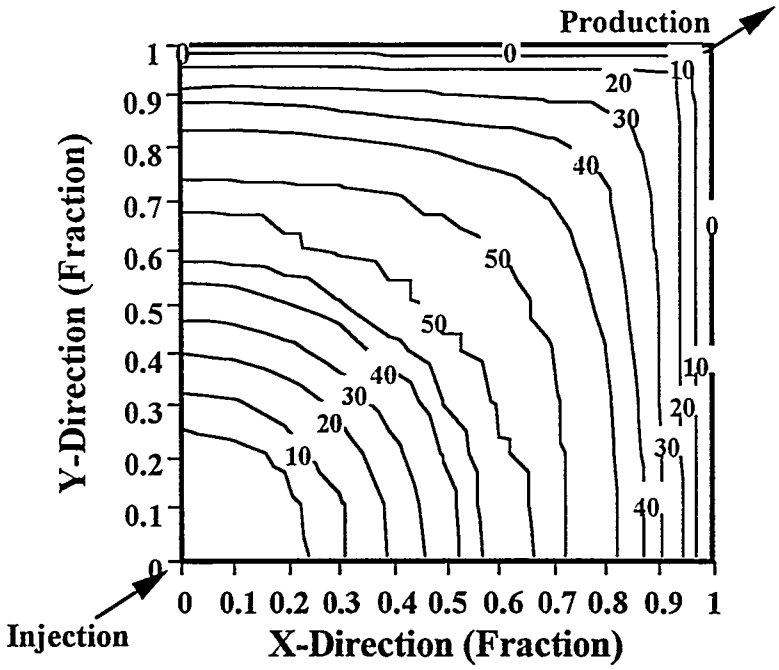

Fig. 18. Water phase viscosity after 1.1 PVs. Injected.

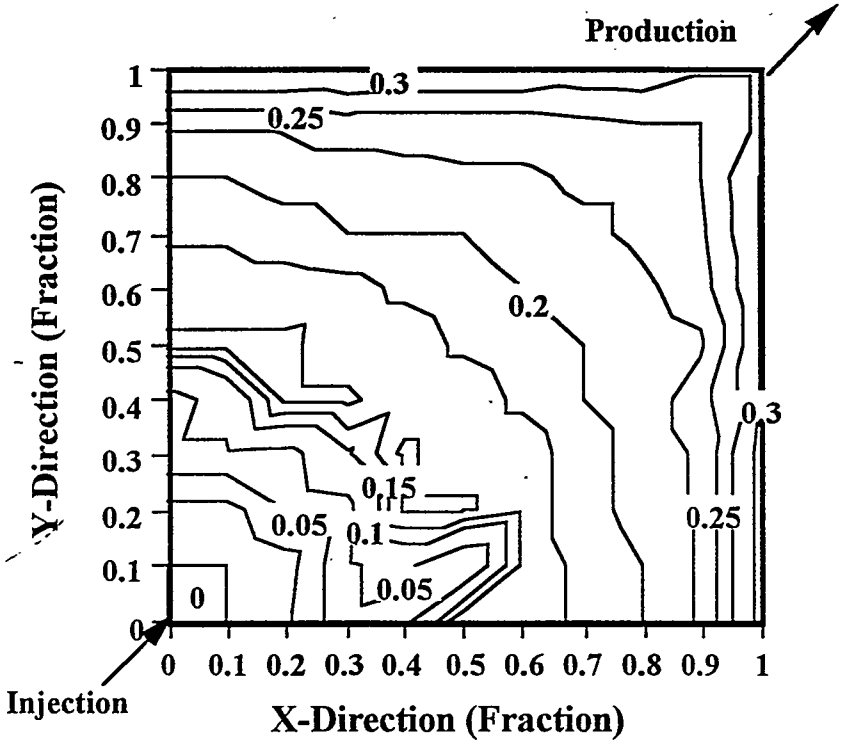

Fig. 19. Oil saturation contour after 1.1 PVs injected.

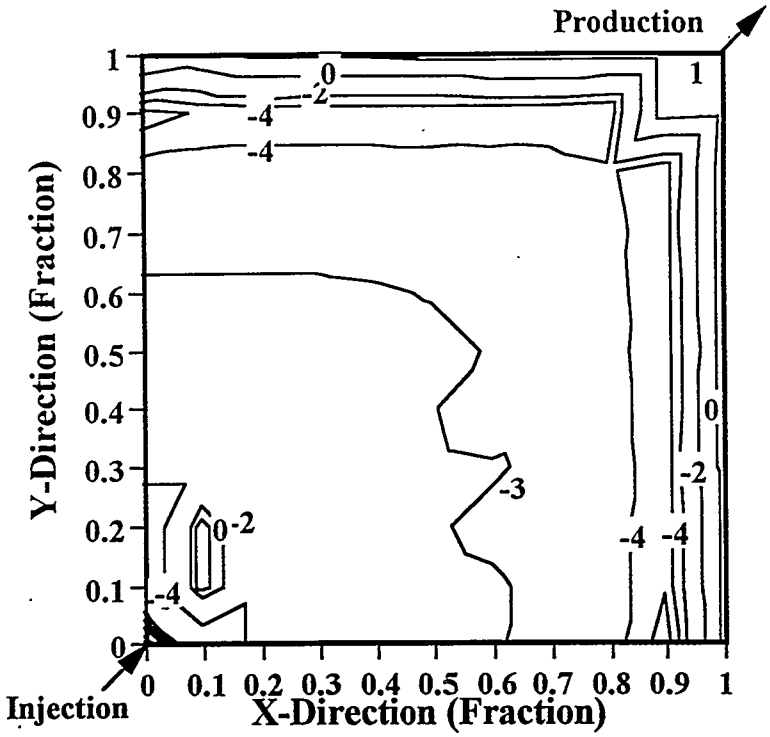

Fig. 20. Log_{10} IFT contour for the water-microemulsion interface (1.1 PV injected).

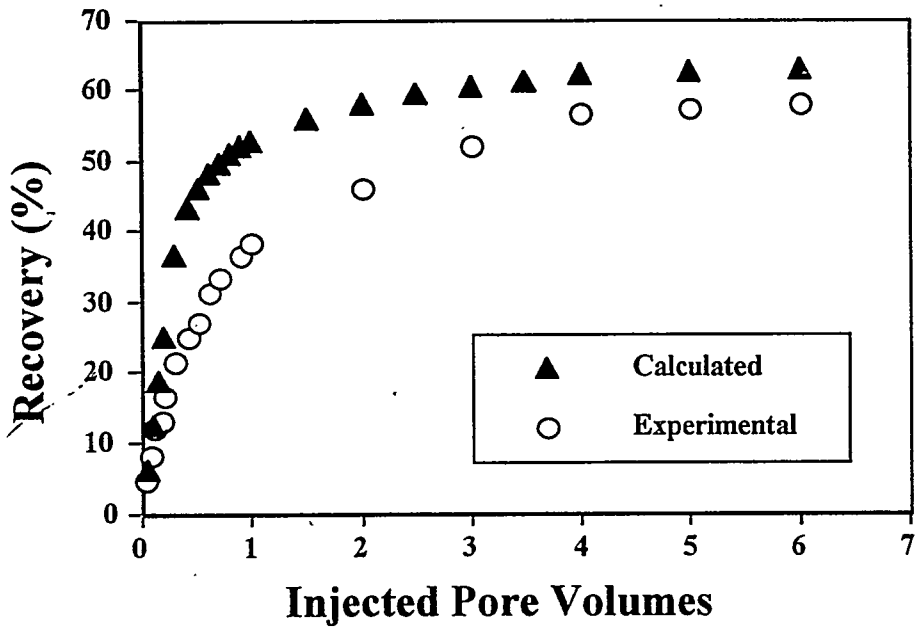

Fig. 21. Comparison between experimental and computed water flood recovery.

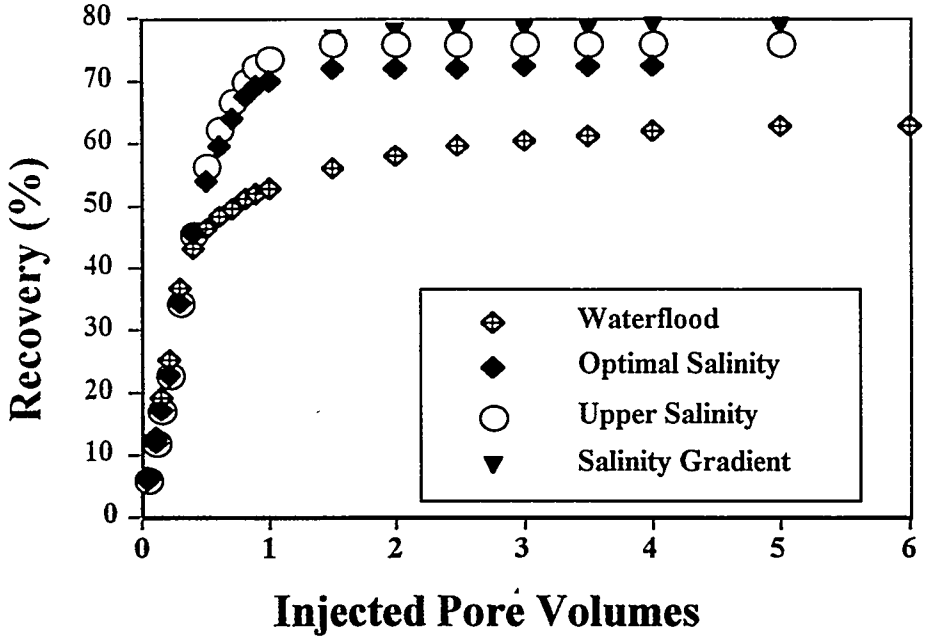

Fig. 22. Influence of salinity on surfactant-polymer recovery.

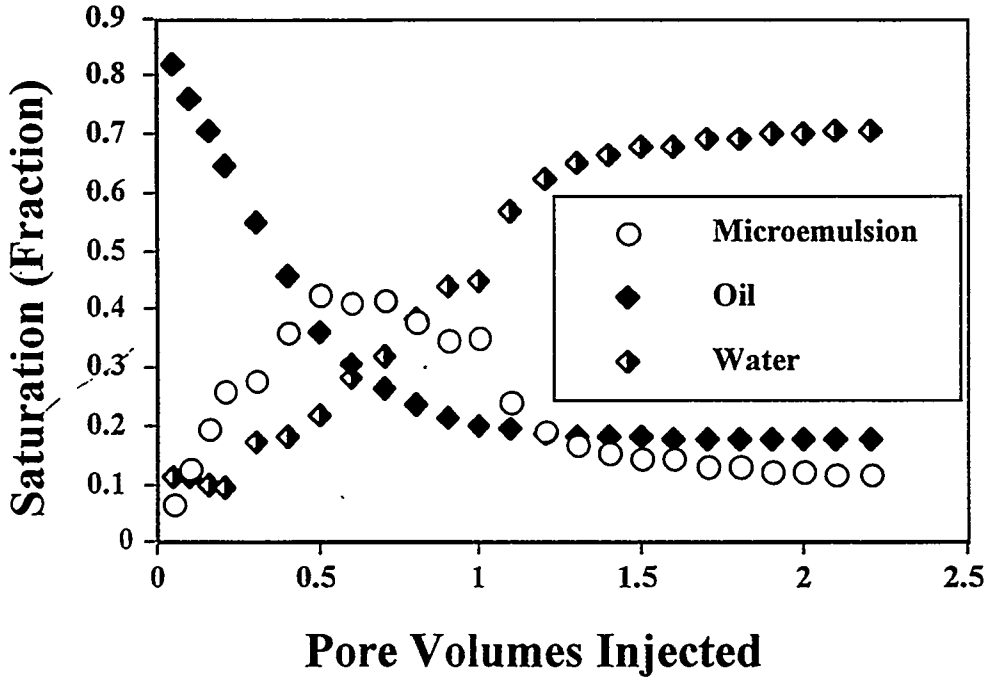

Fig. 23. Average phase saturations time change for optimal salinity.

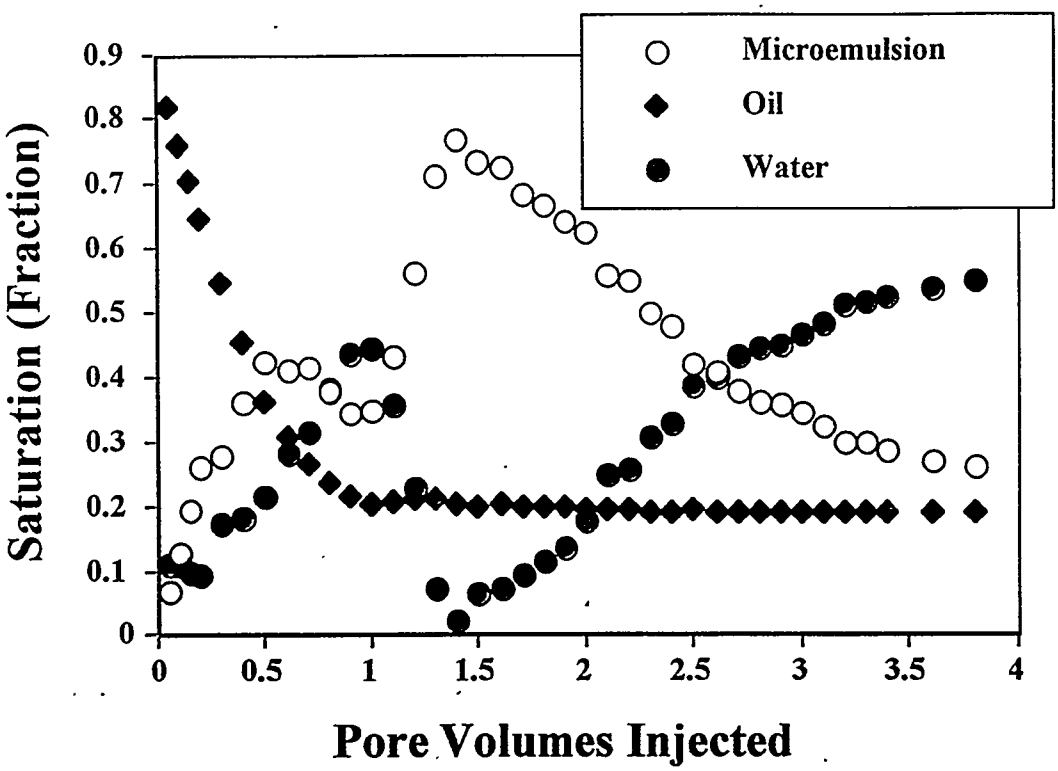

Fig. 24. Average phase saturations time change for salinity gradient.

FUTURE WORK

EXPERIMENTAL PART

Analysis of the data presented in this report has not been completed yet. Some experiments, especially the salinity gradient recovery experiment, will also be completed. It would also be interesting to conduct some floods using a second slug with polymer to see if improved mobility control will reduce (or eliminate fingering). This choice is not economically feasible, but can shed light on the mechanisms proposed in the results section. The addition of co-surfactant to this second slug can help to break the micro-emulsion phase close to the production port. This procedure can mobilize the trapped micro-emulsion phase in the last part of the recovery experiments.

THEORETICAL PROGRAM

Stability Analysis. Results from the stability analysis will be presented for 1-D in next report. The analysis of the 2-D case will continue.

Simulation Program. In order to match the experimental data and theoretical results some heterogeneity will be added to the domain of integration. The idea is to match the water flood recovery curve shown in Fig. 21. In order to do so diagonal permeability bands will be added to the domain. Qualitative agreement with the shape and number of fingers visually determined and successful simulation of the recovery curve will be interpreted as signs of good representation of the experimental behavior of the physical model. After achieving success in this task we will try to match chemical floods where fingering is also present.

ACADEMIC ACTIVITIES

PUBLICATIONS

A paper entitled "Surfactant-Polymer Interaction in Enhanced Oil Recovery" has been published in the Proceedings of the 7th Annual HBCU Energy Symposium. The same material has been presented in the aforementioned Symposium held in Miami, Florida, March 16-18, 1999.

STUDENT ACTIVITIES

Mr. Norman Alban, a graduate student at the Chemical Engineering Department at Prairie View A&M University, will present his Master Thesis entitled "Analysis of Surfactant-Polymer Interaction in Enhanced Oil Recovery" during May, 1999. Mr. Alban work covers the material presented in this, and previous, reports. Mr. Ahmed Noman , another Prairie View A&M University graduate student, will continue working in this research area. Mr. Noman will build a quarter 5-spot apparatus to study selected gel placement in porous media.